Biophysical Journal Volume 98 April 2010 1337–1343

Balanced Electrostatic and Structural Forces Guide the Large Conformational Change Associated with Maturation of T = 4 Virus

Tsutomu Matsui,[†] Hiro Tsuruta,[‡] and John E. Johnson[†*]

[†]Department of Molecular Biology, The Scripps Research Institute, La Jolla, California; and [‡]Stanford Synchrotron Radiation Lightsource, SLAC National Accelerator Laboratory, Menlo Park, California

ABSTRACT *Nudaurelia capensis* omega virus has a well-characterized T = 4 capsid that undergoes a pH-dependent large conformational changes (LCC) and associated auto-catalytic cleavage of the subunit. We examined previously the particle size at different pH values and showed that maturation occurred at pH 5.5. We now characterized the LCC with time-resolved small-angle x-ray scattering and showed that there were three kinetic stages initiated with an incremental drop in pH: 1), a rapid (<10 ms) collapse to an incrementally smaller particle; 2), a continuous size reduction over the next 5 s; and 3), a smaller final transition occurring in 2–3 min. Equilibrium measurements similar to those reported previously, but now more precise, showed that the particle dimension between pH 5.5 and 5 requires the autocatalytic cleavage to achieve its final compact size. A balance of electrostatic and structural forces shapes the energy landscape of the LCC with the latter requiring annealing of portions of the subunit. Equilibrium experiments showed that many intermediate states could be populated with a homogeneous ensemble of particles by carefully controlling the pH. A titration curve for the LCC was generated that showed that the virtual pK_a (i.e., the composite of all titratable residues that contribute to the LCC) is 5.8.

INTRODUCTION

Maturation is an important event associated with establishing virus infectivity (1). It occurs in many complex viruses to accommodate the need for weak interactions between subunits to achieve proper self-assembly and the requirement for a robust particle to survive the extra cellular environment. Maturation results from a program encoded in the initial, often fragile, immature particle that directs large conformational changes resulting in a robust infectious virion. Because purified infectious virions have already achieved the mature state, studies of the maturation process in vitro require the use of virus-like-particles (VLPs) that can be purified in the immature state. Maturation is often triggered by changes in pH or other electrostatic events within the cell allowing in vitro maturation to be controlled by careful adjustment of the pH and the associated state of protonation of critical residues in the capsid. *Nudaurelia capensis* omega virus (NωV) is a highly accessible system for the study of large conformational changes (LCC) leading to particle maturation and associated auto-catalytic subunit cleavage (2).

NωV is a T = 4 icosahedral virus (Fig. 1) that infects *Lepidoptera* (3,4). Expression of the NωV capsid protein gene in a baculovirus system results in the spontaneous formation of VLPs within the infected SF21 cells. When purified at pH 7.6 these particles are ~480 Å in diameter and correspond to the procapsid (5). These particles contain mostly cellular t-RNA and are not infectious. Lowering the pH to 5 in vitro triggers maturation with the particle size reducing to ~400 Å and the initiation of the auto-catalytic cleavage (6). We have shown previously that the size and extent of cleavage are highly sensitive to the pH and can be controlled by carefully adjusting it (2). This sensitivity is due to the negatively charged surfaces of the juxtaposed subunits. At pH 7 the negative charge causes repulsion resulting in the larger size and weak subunit interaction. Indeed, the particle integrity is maintained mostly by subunit interactions with the RNA. At lower pH values the acidic residues are protonated and the repulsion is reduced, as is the particle size. This change is continuous and at a given pH highly homogeneous populations of intermediate sized particles can be produced (6).

We use small-angle x-ray scattering (SAXS) to show that incremental changes in the particle size as a function of pH can be used to determine the overall pK_a of the particle (i.e., a composite of all titratable groups that contribute to the LCC) and that the final stages of the LCC are a delicate balance between electrostatic repulsion and structural resistance imposed before the auto-catalytic cleavage reaction. These studies extend and improve previous equilibrium SAXS measurements with this system (6), allowing the role of subunit cleavage in the LCC to be determined. We also show with time-resolved (TR) SAXS that an incremental reduction in the electrostatic repulsion leads to a collapse of the particle to a smaller size within ~10 ms. This is followed by a continuous change over the next 3–5 s followed by a much slower (~2–3 min) structural reorganization required to achieve the final equilibrium structure at a given pH. The tuning of the different forces analyzed is exquisite, providing an exceptional opportunity for detailed measurements in a nano scale biophysics laboratory.

Submitted October 23, 2009, and accepted for publication December 7, 2009.

*Correspondence: jackj@scripps.edu

Editor: Bertrand Garcia-Moreno.

0006-3495/10/04/1337/7 $2.00

doi: 10.1016/j.bpj.2009.12.4283

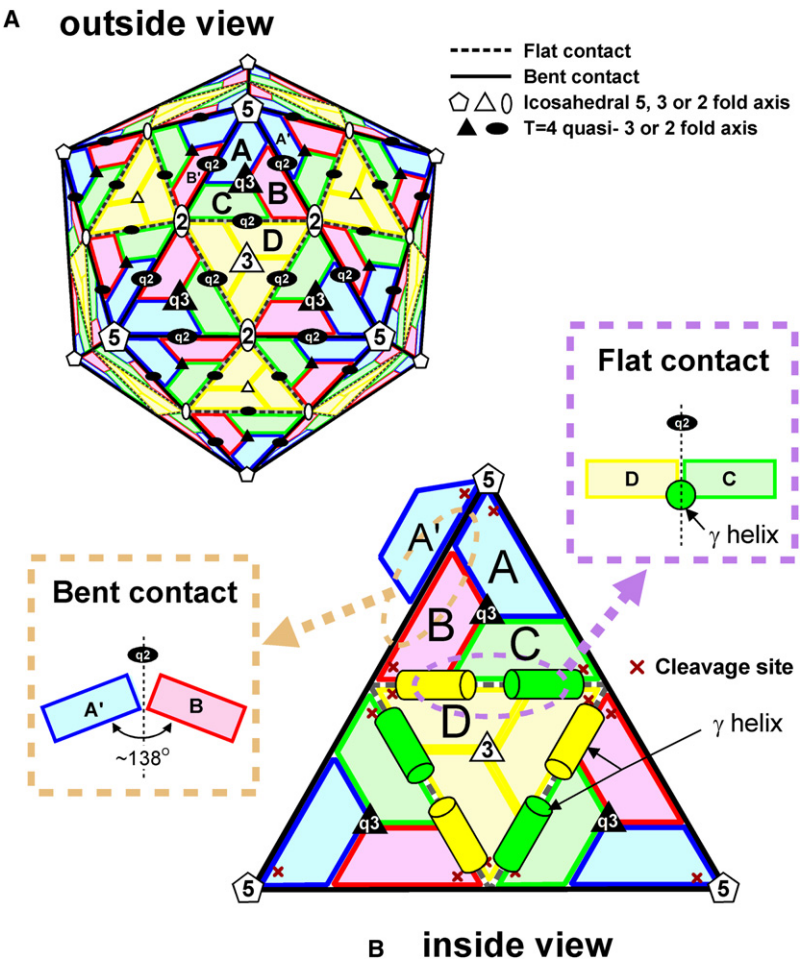

FIGURE 1 A schematic view of the mature T = 4 NωV particle. (*A*) Outside view of the T = 4 subunit arrangement. A particle is composed of 240 coat proteins. The quasi-equivalent A–D subunits (22) share identical sequences but are located in different geometric environments. Based on the dihedral angle between subunits, two classes of subunit-subunit contact are defined. The flat contact of 180° dihedral angle (C-D or B-D) is located along the line between icosahedral twofold axes, whereas the bent contact of ~138° dihedral angle (A′-B, A′-A or B′-C) is located along the line between icosahedral fivefold and twofold axes. (*B*) A schematic view of the subunit interfaces and molecular switches (cylinders) that determine the flat and bent dihedral angles. The view is from inside the particle looking out. The cleavage sites at residue 570 (shown as Xs) generate β (residues 1–570) and γ (residues 571–644) and are located on the interior portion of the shell near the icosahedral fivefold (A subunit) or twofold (quasi sixfold) (B–D subunits) axes. The C-terminal γ helices (residues 613–640) in the C and D subunits function as molecular switches and are observed (i.e., ordered) only at the flat contact where they prevent the hinge motion between subunits and keep the interface flat (17,23).

MATERIALS AND METHODS

Sample preparation

Expression and purification of wt NωV and N570T mutant VLPs have been described (2,7,8). VLPs in the buffer A (10 mM Tris/HCl, pH = 7.6 and 250 mM NaCl) were concentrated to 1.5 mg/mL (wild-type) or 3 mg/mL (N570T). One volume of VLPs solution was added into 2× vol of the buffer B (100 mM NaOAc (for pH = 4.5–5.5) or 100 mM MES (for pH = 5.6–6.8) and 250 mM NaCl). The reaction was incubated at room temperature for designated time. On slow TR experiments, the data collection was exactly started at indicated time. All pH values indicated in figures were confirmed by carrying out the dilutions without VLPs in a volume sufficient to directly measure the pH. VLPs for fast TR SAXS experiment were concentrated to 4 mg/mL in the buffer A. The 1× vol of VLPs solution was mixed with 1 vol of the buffer B using the fast stopped flow mixing device.

Data collection

X-ray scattering measurements in equilibrium and TR modes were conducted at the Beam Line 4-2 of the Stanford Synchrotron Radiation Lightsource (SLAC National Accelerator Laboratory, Menlo Park, CA) in February 2009 and August 2009 (9). The earlier run used a 2.5 m sample-to-detector distance and a MarCCD165 detector (MarUSA, Evanston, IL). A thin-walled quartz capillary cell, maintained at 20°C, kept a sample aliquot in the x-ray beam whose wavelength was calibrated to be 1.127 Å. The ring current ranged from 100 to 78 mA during beam time. The data were collected using 15-μL sample aliquots, employing the data acquisition program Blu-ICE (10,11). Experiments with the wt capsids were performed with 16 successive 2-s exposures. Experiments with N570T capsids were performed with 2 3-s exposures. For each image, an integrated beam intensity value, recorded by a photodiode (International Radiation Detectors, Torrance, CA) mounted inside the beam stop, was used to normalize scattering intensities for small beam intensity variations and different integration times in case of TR experiments. Individual two-dimensional images were scaled, azimuthally integrated, and averaged after inspection for time-dependent variations using the data processing program SASTool (formerly called MarParse) (9). No appreciable change in scattering pattern was detected that would otherwise suggest radiation damage or particle precipitation. Matching blank buffer scattering curves, obtained in the identical way, were subtracted from all virus scattering curves. Detector pixel values were converted to the scattering vector length values $Q = 4\pi\sin(\theta)/\lambda$, where θ is 50% of the scattering angle and λ the x-ray wavelength using the 100 reflection plane and related reflections of a silver behenate powder sample (12). In the later run, additional equilibrium measurements were carried out in the identical way as the earlier run with exception of 1.7-m sample-to-detector distance, a Rayonix MX225-HE CCD detector (Rayonix, Evanston, IL) and 200–148 mA ring current. TR measurements were conducted using a higher beam flux provided by the synthetic multilayer monochromator (13), a stopped-flow rapid mixer, maintained at 20°C, (Unisoku, Hirakata, Japan), and a silicon pixel array detector Pilatus 300K (Dectris, Baden, Switzerland). The estimated mixing dead time of the stopped-flow mixer is 5 ms. The EMBL data acquisition system provided timing pulses required for synchronizing the stopped-flow mixing completion to detector trigger as well as for recording beam integrated intensities synchronously with the series of x-ray scattering measurements (14,15). The following image acquisition sequence

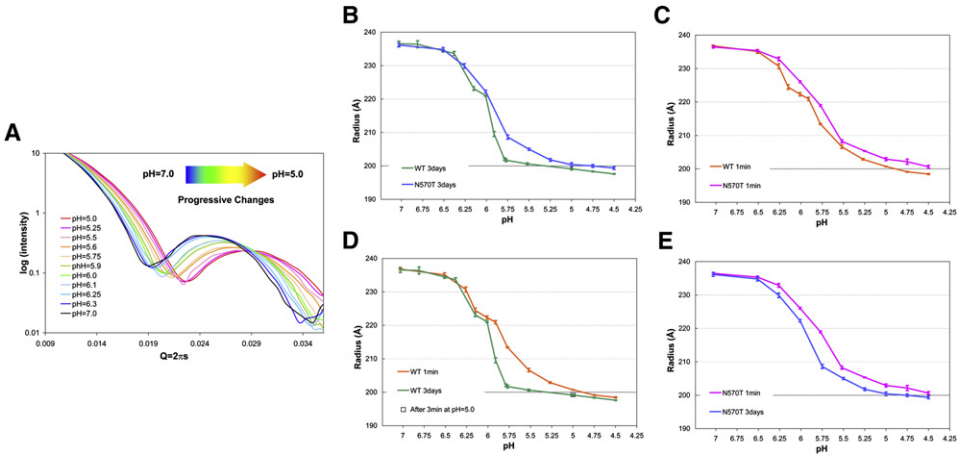

FIGURE 2 (*A*) The progressive changes in the SAXS pattern as a function of pH for wt NωV VLPs. The procapsid particles were incubated at the given pH for 3 days before data collection. The equilibrium SAXS pattern undergoes no further change at that point in time if the pH is carefully maintained. The SAXS data between $Q = 0.009$ and 0.035 $Å^{-1}$, corresponding to a resolution range of 698–179 Å were used for further curve fitting. Note that the change in the SAXS curve is continuous with no ISO scattering points (see Materials and Methods). (*B*) A comparison of the particle radius of the wt NωV VLPs with the N570T noncleaving VLPs after 3days incubation, determined from the equilibrium SAXS curve. The particle radius of the wt NωV VLPs decreases in a continuous manner between pH 6.5 and 5.5 with the midpoint at pH 5.8. We interpret this plot as a titration curve for the overall particle, thus the pK_a for the particle corresponds to the midpoint position. The curves superimpose within experimental error between pH 7.0 and 6.0. Between pH 6.0 and 5.0 the differences in the radii are significantly greater than the experimental error. The wild-type particles initiate auto-catalytic cleavage at pH 5.8 where ~30% of the subunits cleave in 3 days. At pH values of 5.5 and below virtually 100% of the subunits cleave in 3 days. Between pH 5.75 and 5.25, cleavage is important for the final size of the particle. There is a balance of forces between electrostatic repulsion and resistance to condensation due to the uncleaved subunit polypeptides. At pH 5 and below the reduction in electrostatic repulsion overcomes any effect of subunit cleavage. (*C*) A curve similar to that shown in *B*, except incubation times before the size measurement were only 1 min. In contrast to *B*, in this time regime, the two curves are closely similar at all pH values. Because even at pH 5.0, very little cleavage has occurred in 1 min, this plot supports the role of cleavage in allowing particle condensation. (*D*) A comparison of 1 min and 3 day incubations for wt VLPs. The plot emphasizes the role of annealing and cleavage in achieving the final particle size. Between pH values of 7.0 and 6.0 there is no cleavage at any time point. We interpret the difference in particle size as the time required for the subunit polypeptide to anneal sufficiently to achieve the minimum radius. Between pH 5.8 and 5.0 subunit cleavage is a dominant factor in the particle condensation. Time resolved studies of the wt VLPs radius after 3 min at pH 5.0 show that in that time frame sufficient cleavage has occurred to allow particle condensation. (*E*) A comparison of N570T incubated for 1 min or 3 days at the pH values indicated. Here there is no effect of cleavage so the differences in radii at the two time points must be due to subunit annealing alone.

was used for each mixing event: 64 images with 7-ms integration, 64 images with 27-ms, 32 images with 97-ms, and 16 images with 297-ms. Each image acquisition is followed by 3-ms readout. The first image thus covered between 5 and 12 ms after the reaction initiation (taking into account 5 ms mixing dead time), the second image 15 and 22 ms, and so on.

Curve fitting

All SAXS patterns were analyzed with the routine *MIXTURE* within the software suite *PRIMUS* (12). A polydisperse solid sphere with a uniform density was fit for this type of analysis. Interparticle interactions were not taken into account and the radius and the polydispersity defined by a monomodal Gaussian distribution were parameterized. Scattering below the second maximum ($Q < 0.035$) was used for curve fitting. The results of the equilibrium and slow TR experiments were based on the average (±SD) of three independent experiments.

RESULTS

SAXS data were collected in both equilibrium (static) and TR modes to study the LCC of the capsid during the maturation of NωV. Equilibrium experiments were carried out at pH values between 7.0 and 4.5 at different intervals, depending on the pH range. Data were collected with 3-s exposure times and analyzed in the range from $Q = \sim 0.01$ to 0.035 $Å^{-1}$. In each case the particles were incubated at the given pH for 3 days (see Materials and Methods) with no further change in the SAXS pattern observed during longer incubations, thus the particles were in a static conformation after this period of incubation. Fig. 2 *A* shows the progressive change in the SAXS pattern as the pH was lowered at the intervals indicated. There were no indications of ISO scattering points in the pattern indicating that the particles changed size in a continuous manner and that the ensemble of particles was nearly homogeneous. We evaluated the particle size by a curve fitting procedure in which the particle radius and polydispersity were the only two parameters describing the uniform density sphere model (16). The procedure allows the particle radius to be estimated with a precision of ~2 Å (see Fig. S1 *A* in the Supporting Material). The polydispersity of all the equilibrium measurements is virtually constant ($\sigma = \sim 0.5\%$) at all pH values for experiments carried out under identical conditions (see Fig. S1 *B*). The average value of the polydispersity, however, changes from ~14% for wt measurements to ~23% for the N570T mutant measurements. As these data were measured under different experimental conditions (e.g., different detectors were used at different specimen to detector distances), we believe that the polydispersity accounts for insufficient resolution of the zero points in the spherical diffraction pattern and that the actual dispersity in particle size is significantly less than the percentage indicated in the curve fitting. This is supported by the subnanometer cryo-electron microscopy (cryo-EM) reconstructions of the NωV

procapsid and capsid recently reported and the close similarity between these extreme SAXS curves and those of intermediate size (17).

Fig. 2 *B* shows the estimated particle radius at equilibrium of the wt NωV and the N570T mutant as a function of pH, determined with the curve-fitting procedure. Measurements of the wild-type particle at pH 7.0 and 6.8 displayed virtually identical patterns (corresponding to a radius ~236 Å) indicating no effect on the particle diameter in this range of pH. The first detectable change in the particle radius occurred at pH 6.5 where it decreased by ~2.8 Å. Between pH 6.5 and 5.5 the particle radius changes by 35 Å in a continuous manner, with a value of 201 Å at pH 5.5. Only a small reduction in size is observed between pH 5.5 and 4.5 with a final radius of 197 Å. This curve corresponds to the titration of acidic residues and shows that the overall experimental pK_a for the particle is ~5.8.

The N570T mutation, that does not undergo the maturation cleavage, shows identical behavior to wt at pH values between 7 and 6.0. However, they separate at pH values between 5.8 and 5, with the mutant particle displaying systematically larger radii above pH 5.0. Below this pH the two particle dimensions are closely similar, but the mutant is systematically larger and this may result from the inability of the threonine to properly pack at the active site normally occupied by the asparagine.

The difference in particle size between pH 5.8 and 5 is due likely to the effect of cleavage in the wild-type particle. To test this hypothesis a second experiment with wild-type and N570T VLPs was carried out in which they were incubated for exactly 1 min before 3 s data collection. This incubation time was chosen because at pH 5.5, virtually no cleavage occurs in 1 min (2), thus wt and N570T would be expected to display very similar curves at this pH if the differences observed in the long incubation were due to cleavage. Fig. 2 *C* shows that the wt and N570T titration curves recorded after a 1-min incubation have closely similar shapes over the entire pH range, although the wt particle is systematically slightly smaller and there is no significant drop between pH = 6 and 5, confirming the role of cleavage in the LCC. Fig. 2 *D* confirms the role of cleavage by comparing the wt particle radii at 1 min and 3 days showing the dramatic effect of cleavage between 6.0 and 4.75. At pH 5 data were collected after a 3-min incubation, at which point ~15% of the subunits are cleaved, and the particle size is already identical to the 3-day incubation indicating that only a small fraction of the subunits need to cleave to achieve the final particle conformation.

The experimental results above show clearly that cleavage is required for the full LCC at pH 5.5. We interpret this as an adaptation of the subunit interfaces that depends on cleavage. However, examination of Fig. 2 *E* suggests that other adjustments dependent on pH, but not cleavage, occur at all pH values between 6.5 and 4.75 with the most dramatic difference in the LCC occurring at pH 5.75.

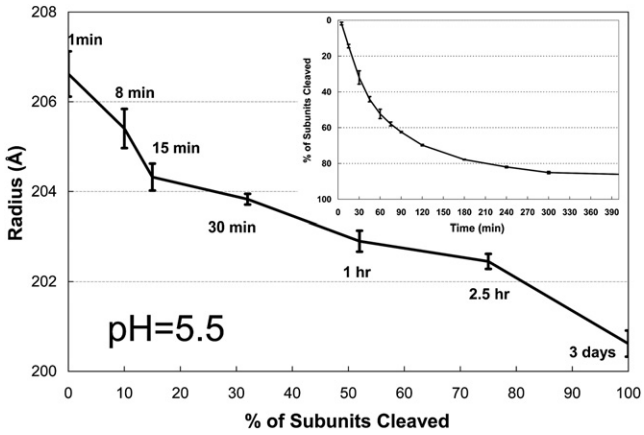

FIGURE 3 A TR analysis of the wt VLP at pH 5.5. The particle radius decreases from 236 to 207 Å in 1 min (see Fig. 4 *A*) and then slowly decreases in size to ~200 Å as shown. The size change is closely proportional to the fraction of subunits cleaved, emphasizing the role of cleavage at this pH in the final stages of particle condensation. The kinetics of particle cleavage at pH 5.5 is shown in the inset graph (2).

To directly determine the relationship between cleavage and particle size, a TR experiment was carried out at pH 5.5 (the maximum pH at which 100% cleavage occurs in 3 days), near where the greatest difference between the 1-min time point and the 3-day time point occurred. Fig. 3 shows that the particle size changes with the percent cleavage and at this pH virtually 100% of the subunits must be cleaved to reach the size of the mature capsid.

The various changes to the particle described at pH 5.5 all occurred after the dramatic size reduction from 236 to 207 Å. The rate at which this large change occurs was studied as a function of pH with TR SAXS. The maximum time resolution for the experiment is ~10 ms and these frames were recorded after the drop in pH using a stop-flow mixing apparatus. Fig. 4 *A* shows the dependence of particle size on pH from 12 ms to 3 days. The rate of the LCC is similar in the first ~20 ms at pH values between 6 and 4.5, however, the initial particle size after the drop in pH is significantly smaller at the lower pH values in this time regime (Fig. 4, *B* and *C*). Fig. S2 *B* shows a detailed description of the changes in particle size during the first second at the designated pH value. The data show that the rate at which the initial smaller size is achieved is very rapid in each case, however, as in the longer time regime measurements, there is a subsequent annealing time required to fully achieve the final size at a given pH.

DISCUSSION

NωV has evolved a remarkable electrostatic environment that allows a controlled maturation from procapsid to mature capsid. Cellular apoptosis has been proposed as the biological driving force for this maturation, as cells in their final

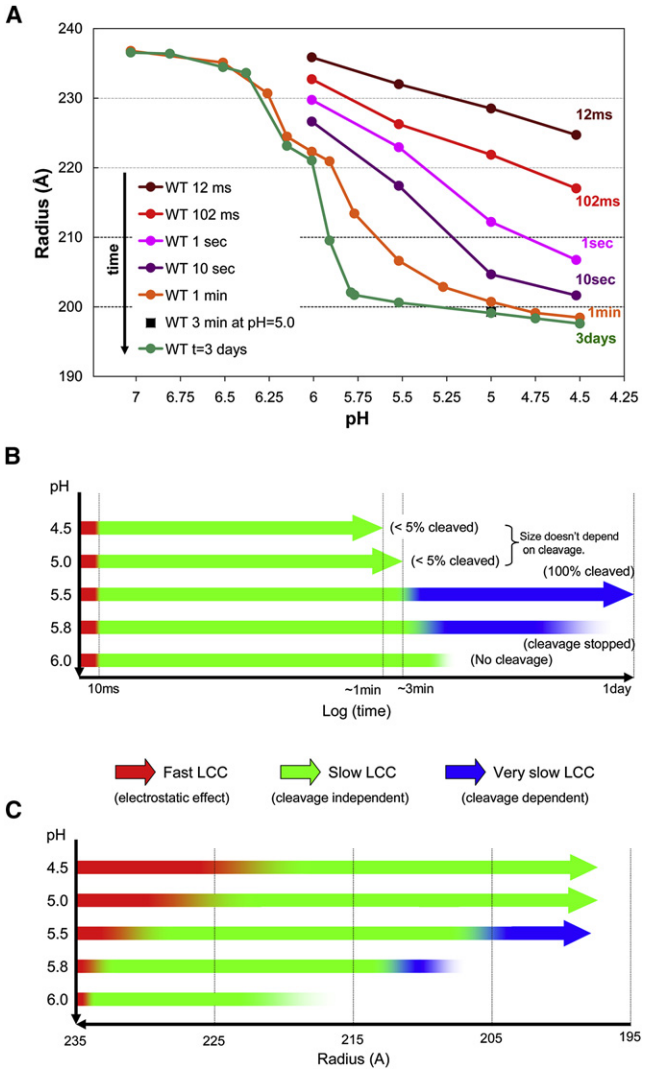

FIGURE 4 A summary illustrating the temporal and spatial components of the NωV particle LCC change. (*A*) A TR analysis between 12 ms and 3 days of the particle dimension at pH values between 7 and 4.5. At pH 6 there is a size reduction from 236 to 222 Å in 1 min with three intermediate-sized particles resolved between 12 ms and 10 s (Fig. S2). Between pH 5.5 and 4.5 particles condense from 236 to 231–225 Å in 12 ms or less. Those sizes must be where the first resistance to condensation is met, initiating the pH-dependent annealing resulting in additional intermediates, that are progressively smaller at lower pH values and readily detected at time points between 102 ms and 10 sec. (*B*) A plot illustrating the time frame for different events associated with the LCC at different pH values. At all pH values below 6.0 there is a rapid condensation within ~10 ms (*red*), the extent of which depends on pH (see *B* and Fig. S2). There is minimal resistance to the subunit condensation during this first change. The first resistance to subunit condensation is overcome by polypeptide and possibly RNA annealing that occurs between 10 ms and ~5 min leading to the initiation of auto-proteolysis. Note that at pH 6.0 and above there is annealing in this time frame, but cleavage is never initiated. The next stage of condensation resistance (that only occurs between pH 5.0 and 5.8) is overcome by the subunit cleavage and this occurs between 3 min and 1 day (e.g., see Fig. 3). (*C*) A plot that correlates size change with the time regimes shown in *B*. In the pH range of 4.5–5.0 the first resistance to condensation occurs at 224–228 Å correlating with a size change of 8–12 Å in 10 ms. Between pH 5.8 and 6.5 a change of only 2–3 Å occurs in the same time interval.

stage of existence display a lower pH than healthy cells (18,19). Thus NωV assembly and RNA packaging occurs at pH 7 where subunit interactions are tenuous due to electrostatic repulsion and differences between quasi-equivalent interactions are minimized. The lower pH of apoptotic cells reduces the repulsion and induces maturation.

We have characterized the details of the size dependence of NωV on pH as well as the rate of subsequent adaptations of subunit interfaces required for the full particle maturation. At pH 5.5 there is sufficient remaining electrostatic repulsion that full maturation depends on the auto-catalytic cleavage. Fig. 3 provides a striking relationship between the fraction of subunits cleaved and the particle size at this pH. In contrast the particle minimizes its size at pH 5 and below, even without the cleavage. Thus, there is a delicate balance between electrostatic repulsion and strain induced by the uncleaved tertiary structure. Whereas the wt NωV reduces this strain with cleavage, the N570T mutant permanently stops at the premature particle size at pH 5.5. This balance of structural resistance to particle size reduction is readily overcome at pH 5 where all particles, regardless of their state of cleavage, have nearly identical sizes.

The TR SAXS data show that at pH values <6, the particle size collapses to a reduced dimension within 10 ms and then the size continues to decrease in a continuous manner for the next 5 s. A much slower and smaller size reduction occurs in the next 2–3 min. This, we believe, is dependent on slow reorganization of portions of the subunit involved in molecular switching and possibly autocatalysis. The time regime of this latter transition and the homogeneity of the particles suggest that three-dimensional information could be obtained for these transitions with TR (3 min to 4 h) cryo-EM. These experiments are currently underway. Fig. 4, *B* and *C*, summarizes the temporal and spatial behavior of the particles between pH 6.0 and 4.5.

We reported previously the cryo-EM reconstruction of a mutant of NωV (E278Q) that could not undergo the full LCC at pH 5.0 in the normal time frame (the transition that normally occurs in ~2 min required nearly 8 h) and this provided some mechanistic insight into one aspect of the adaptations that must be achieved for the full LCC change (2). The spherically averaged radius of the E278Q particle at pH 5.0 was 207 Å, a dimension normally observed for particles at pH 5.75 at the 2-min incubation time. No cleavage for the E278Q particles was detected until

At pH values between these two extremes have size changes roughly proportional to the pH. The number of annealing events and the effect of these on particle size are highly dependent on pH. Between pH 4.5 and 5.0 noncleavage-dependent annealing is readily measurable in the 10 ms to 3 min time frame, but cleavage is not required at all to reach the fully condensed state. In contrast at pH 5.5 noncleavage-dependent annealing is measured between 10 ms and 5 min and cleavage-dependent annealing occurs between 5 min and 1 day. At pH 5.8 the fully condensed state is never reached because the required cleavage stops at ~12 h with only ~30% subunit cleaved. (See Supporting Material for details of the TR analysis.)

~30 min after pH reduction. The pseudo-atomic model for this intermediate sized particle showed that side chains of residue 278, located near the threefold and quasi-threefold axes, made a lock and key interaction on size reduction that was inhibited when *Q* replaced *E*. We propose that in the wt NωV this insertion occurs in ~1 min and contributes to the annealing time observed at pH 5.5.

The effect of cleavage on the particle size can be rationalized from recent subnanometer cryo-EM reconstructions of the wt, fully mature capsid at pH 5.0, and the capsid of N570T (noncleaving mutant) at pH 5.0. The major difference in the electron density occurred at residues 613–640 of the C and D subunits where that polypeptide was well ordered in the wt particle and disordered in the N570T particle (17). These residues function as a molecular switch that controls the angle at the subunit interface between the B-C subunits and D-D subunits (Fig. 1). Cleavage allows these residues to fully insert at this interface whereas they remain dynamic before cleavage. At the pH of the cryo-EM reconstructions the size of the two particles is closely similar in agreement with the SAXS measurements of the two particle types at pH 5 that are also the same within experimental error. However, at pH 5.5, cleavage is required to complete the LCC. N570T never completes the LCC at this pH and Fig. 3 shows that there is a strong correlation between particle size and the fraction of subunits cleaved. We propose that the particle size change directly reflects the organization of residues 613–640 and their ordering into the subunit interface as the cleavage relaxes constraints on the tertiary structures of these polypeptides.

The mechanism evolved for NωV maturation has produced a nano physics laboratory in which molecular driving forces can be controlled and balanced readily. The continuous nature of the particle transition, where numerous intermediate states can be populated in a homogenous manner, together with the high resolution x-ray model and numerous subnanometer cryo-EM reconstructions allows the rational design of mutations that may trap intermediate forms of the particle for further biophysical analysis. The behavior of the particles determined in this and previous studies suggests that a kinetically characterized NωV mutation (E73Q) will allow such an intermediate structure to be trapped and characterized (2).

The continuous nature of the NωV pH dependent maturation is strikingly different from another well-characterized maturation observed in the bacteriophage HK97 (20) HK97 maturation depends on a metastable particle achieved through scaffold-protein mediated assembly and subunit proteolysis catalyzed by a virally encoded protease (21). On DNA packaging this particle proceeds through an exothermic maturation cascade dramatically increasing its diameter with no populated intermediate particles. Thus, although the necessity for maturation seems universal in complex virus assembly the mechanistic details are markedly different.

SUPPORTING MATERIAL

Two figures are available at http://www.biophysj.org/biophysj/supplemental/S0006-3495(09)06101-3.

Stanford Synchrotron Radiation Lightsource is operated by Stanford University for the United States Department of Energy, Office of Basic Energy Sciences.

This work was supported by the National Institutes of Health (GM54076 to J.E.J). The SSRL Structural Molecular Biology Program is supported by the United States National Institutes of Health, National Center for Research Resources (RR001209), and by the Department of Energy Office of Biological and Environmental Research.

REFERENCES

1. Steven, A. C., J. B. Heymann, …, J. F. Conway. 2005. Virus maturation: dynamics and mechanism of a stabilizing structural transition that leads to infectivity. *Curr. Opin. Struct. Biol.* 15:227–236.
2. Matsui, T., G. Lander, and J. E. Johnson. 2009. Characterization of large conformational changes and autoproteolysis in the maturation of a T = 4 virus capsid. *J. Virol.* 83:1126–1134.
3. Hanzlik, T. N., and K. H. Gordon. 1997. The *Tetraviridae*. *Adv. Virus Res.* 48:101–168.
4. Speir, J., and J. Johnson. 2008. Tetravirus structure. *In* Encyclopedia of Virology, 3rd ed. Elsevier, Oxford. 27–37.
5. Canady, M. A., M. Tihova, …, M. Yeager. 2000. Large conformational changes in the maturation of a simple RNA virus, *Nudaurelia capensis* omega virus (NomegaV). *J. Mol. Biol.* 299:573–584.
6. Canady, M. A., H. Tsuruta, and J. E. Johnson. 2001. Analysis of rapid, large-scale protein quaternary structural changes: time-resolved X-ray solution scattering of *Nudaurelia capensis* omega virus (NωV) maturation. *J. Mol. Biol.* 311:803–814.
7. Taylor, D. J., and J. E. Johnson. 2005. Folding and particle assembly are disrupted by single-point mutations near the autocatalytic cleavage site of *Nudaurelia capensis* omega virus capsid protein. *Protein Sci.* 14:401–408.
8. Taylor, D. J., N. K. Krishna, …, J. E. Johnson. 2002. Large-scale, pH-dependent, quaternary structure changes in an RNA virus capsid are reversible in the absence of subunit autoproteolysis. *J. Virol.* 76:9972–9980.
9. Smolsky, I. L., P. Liu, …, H. Tsuruta. 2007. Biological small-angle x-ray scattering facility at the Stanford synchrotron radiation laboratory. *J. Appl. Cryst.* 40:S453–S458.
10. Reference deleted in proof.
11. McPhillips, T. M., S. E. McPhillips, …, P. Kuhn. 2002. Blu-Ice and the distributed control system: software for data acquisition and instrument control at macromolecular crystallography beamlines. *J. Synchrotron Radiat.* 9:401–406.
12. Huang, T. C., H. Toraya, …, Y. Wu. 1993. X-ray-powder diffraction analysis of silver behenate, a possible low-angle diffraction standard. *J. Appl. Cryst.* 26:180–184.
13. Tsuruta, H., S. Brennan, …, K. O. Hodgson. 1998. A wide-bandpass multilayer monochromator for biological small-angle scattering and fiber diffraction studies. *J. Appl. Cryst.* 31:672–682.
14. Khazaie, J. B., and C. Boulin. 1996. An 8-channel counter and histograming sub-module: the basic building block for fast real-time data acquisition systems. *IEEE Trans. Nucl. Sci.* 43:193–196.
15. Khazaie, J. B., and C. Boulin. 1996. Time frame generator for x-ray detectors and data acquisition systems for synchrotron radiation applications in molecular biology. *IEEE Trans. Nucl. Sci.* 43: 197–201.
16. Konarev, P. V., V. V. Volkov, …, D. I. Svergun. 2003. PRIMUS: a Windows PC-based system for small-angle scattering data analysis. *J. Appl. Cryst.* 36:1277–1282.

17. Tang, J., K. K. Lee, …, J. E. Johnson. 2009. Dynamics and stability in maturation of a T = 4 virus. *J. Mol. Biol.* 392:803–812.

18. Brooks, E. M., K. H. Gordon, …, T. N. Hanzlik. 2002. Infection of its lepidopteran host by the *Helicoverpa armigera* stunt virus (*Tetraviridae*). *J. Invertebr. Pathol.* 80:97–111.

19. Tomasicchio, M., P. A. Venter, …, R. A. Dorrington. 2007. Induction of apoptosis in *Saccharomyces cerevisiae* results in the spontaneous maturation of Tetravirus procapsids in vivo. *J. Gen. Virol.* 88:1576–1582.

20. Lee, K. K., H. Tsuruta, …, J. E. Johnson. 2005. Cooperative reorganization of a 420 subunit virus capsid. *J. Mol. Biol.* 352:723–735.

21. Gertsman, I., L. Gan, …, J. E. Johnson. 2009. An unexpected twist in viral capsid maturation. *Nature.* 458:646–650.

22. Caspar, D. L., and A. Klug. 1962. Physical principles in the construction of regular viruses. *Cold Spring Harb. Symp. Quant. Biol.* 27:1–24.

23. Helgstrand, C., S. Munshi, …, L. Liljas. 2004. The refined structure of *Nudaurelia capensis* omega virus reveals control elements for a T = 4 capsid maturation. *Virology.* 318:192–203.